Journal of Power Sources 271 (2014) 32–41

Contents lists available at ScienceDirect

Journal of Power Sources

journal homepage: www.elsevier.com/locate/jpowsour

Hydrogen storage reactions on titanium decorated carbon nanocones theoretical study

A.S. Shalabi [a, *], H.O. Taha [b], K.A. Soliman [a], S. Abeld Aal [a]

[a] Department of Chemistry, Faculty of Science, Benha University, P.O. Box 13518, Benha, Egypt
[b] Department of Physics, Faculty of Education, Ain Shams University, Cairo, Egypt

HIGHLIGHTS

- DFT study of hydrogen storage on Ti functionalized CNC.
- Ti can bind up to 6 hydrogen molecules with surface coverage 0.94.
- Reversible and irreversible reactions are characterized.
- Expected hydrogen storage capacity 14.34 wt% and rate constants ratio 1.35.
- Physisorption and thermodynamics meet the ultimate targets of DOE for vehicle operation.

ARTICLE INFO

Article history:
Received 24 March 2014
Received in revised form
28 June 2014
Accepted 23 July 2014
Available online 1 August 2014

Keywords:
Density functional theory
Hydrogen storage
Titanium complexes
Carbon nanocones

ABSTRACT

Hydrogen storage reactions on Ti decorated carbon nanocones (CNC) are investigated by using the state of the art density functional theory calculations. The single Ti atom prefers to bind at the bridge site between two hexagonal rings, and can bind up to 6 hydrogen molecules with average adsorption energies of −1.73, −0.74, −0.57, −0.45, −0.42, and −0.35 eV per hydrogen molecule. No evidence for metal clustering in the ideal circumstances, and the hydrogen storage capacity is expected to be as large as 14.34 wt%. Two types of interactions are recognized. While the interaction of $2H_2$ with Ti–CNC is irreversible at 532 K, the interaction of $3H_2$ with Ti–CNC is reversible at 392 K. Further characterizations of the former two reactions are considered in terms of projected densities of states, simulated infrared and proton magnetic resonance spectra, electrophilicity, and statistical thermodynamic stability. The free energy of the highest hydrogen storage capacity reaction between $6H_2$ and Ti–CNC meets the ultimate targets of department of energy at (233.15 K) and (11.843 atm) with surface coverage (0.941) and (direct/inverse) rate constants ratio (1.35).

1. Introduction

Hydrogen powered fuel cell is a technology being pursued as an alternative to gasoline. As an energy carrier for use in vehicle applications, hydrogen has several advantages. It has the highest density by weight and can be produced renewably. In this direction a wide range of materials are currently being considered as potential reversible hydrogen storage materials. Of these, carbon based materials can be structured into a variety of forms including carbon nanotubes, fibers, fullerenes, and activated carbons. They are attractive materials for hydrogen storage, as they have the potential to be low cost, light weight, reversible, and possess facile hydrogen charge–discharge kinetics. However, they share a common limitation of weak van der Waals interaction between molecular hydrogen and the host material which is translated to an operating temperatures at or near that of liquid nitrogen. Therefore, to enhance hydrogen binding, small amounts of hydrogen dissociating catalysts such as transition metals are added to generate atomic hydrogen.

The hydrogen sorption properties of carbon nanotubes have been investigated extensively in recent years. However, there has been considerable controversy over the storage properties of some of these materials since the publication of the first report of the potential for room temperature storage of hydrogen by carbon nanotubes [1]. The results for hydrogen storage in carbon nanotubes have led to the emergence of carbon nanohorns. Single walled carbon nanohorns (SWCNHs) consist of single walled

* Corresponding author. Tel.: +20 2 24188738, +20 100 5211681(mobile); fax: +20 2 24188738.
E-mail address: asshalabi@hotmail.com (A.S. Shalabi).

http://dx.doi.org/10.1016/j.jpowsour.2014.07.158
0378-7753/

graphitic structures formed out of a single graphene sheet rolled up to form conical (horn like shapes), that aggregate to form globular rosette structures with sizes of about 80–100 nm. CNHs exhibit very large surface areas approaching 1500 $m^2\ g^{-1}$. Because of low cost, high purity and high surface area CNHs became attractive candidates for hydrogen storage. Heats of adsorption corresponding to 100–120 meV have been reported and attributed to enhanced interaction of H_2 molecules at the conical tip of nanohorn [2].

CNHs are subclass of the carbon nanocones CNCs family. They are the fifth allotropic form of carbon, and have been selected for investigating hydrogen storage capacity because initial temperature programmed desorption experiments found a significant amount of hydrogen was evolved at ambient temperatures [3]. However, hydrogen storage on CNCs has been relatively little explored theoretically. Ming-Liang Liao [4] investigated hydrogen adsorption behaviors of single walled carbon nanocones SWCNCs by molecular dynamics simulations. A. Gotzias et al. [5] examined hydrogen adsorption on CNHs and CNCs by using the grand canonical Monte Carlo method. Q. Wang et al. [6] tested the capability to store hydrogen by using the gradient corrected density functional theory.

Yildirim and Ciraci [7] investigated Ti decorated CNT as potential high capacity hydrogen storage medium. They found that the first H_2 adsorption is dissociative, while other adsorptions are molecular with elongated H–H bonds in agreement with our results for Ti decorated CNC. However, they reported that Ti binds up to four hydrogen molecules with hydrogen storage capacity up to 8 wt% in contrast with our results that Ti binds up to six hydrogen molecules with expected hydrogen storage capacity up to 14.34 wt%. These discrepancies might be attributed to the different curvatures of CNTs and CNCs. Samolia and Kumar [8] carried out theoretical calculations to examine the hydrogen sorption efficiency of Ti functionalized MOF with organic linker replaced with BN linker. They reported that low adsorption and desorption energies suggest the high hydrogen reversibility of the system. This may be correlated with the present reversible adsorption energies of 3–6 H_2 molecules relative to the irreversible adsorption energies of 1 and 2 H_2 molecules. They also reported that Ti adsorbs 4 H_2 molecules by Kubas interaction with average desorption temperature 323 K and storage capacity 7.8 wt%. This desorption temperature may be compared with the present 233.15 K assigned for the highest hydrogen storage capacity reaction between $6H_2$ and Ti–CNC. The preferred orientation of single H_2 molecule adsorbed on Ti decorated CNT was investigated by Shalabi et al. [9]. The preferential adsorption of H_2 was found to be on Ti atom located on the most stable top adsorption site of the (5,5) SWCNT, with H_2 oriented parallel to tube (x)-[100] axis. The corresponding adsorption energy of −0.44 eV meets the DOE target for physisorption (−0.2 to −0.6 eV) and is close to the present average adsorption energy of $4H_2$ molecules (−0.45 eV). Carbon based materials decorated by transition metals other than Ti have been also investigated. Nachimuthu et al. [10] found that among the investigated transition metals, the Ni, Pd and Co atoms were suitable for decorating boron doped graphene, which could be adsorbed stably on the surface. They reported −0.68 eV for single hydrogen molecule adsorption on Pd. This value may be compared with the results of Xiao et al. [11]. They reported 0.80 eV for single hydrogen molecule adsorption on Pd with bond direction perpendicular to the axis of the (8,0) SWCNT. They also reported that electrostatic Coulomb attraction and orbital repulsion mediate the interaction between H_2 and Pd.

Hydrogen storage in Yttrium decorated single walled carbon nanotube has been investigated by Chakraborty et al. [12]. They predicted that a single Y atom attached on SWCNT can adsorb up to six hydrogen molecules and showed that 100% desorption at comparatively lower temperature can be achieved in a transition metal decorated SWCNT system. Finally, J. Yang et al [13] reviewed the most valuable experimental and computational techniques employed in the field of hydrogen storage materials research.

With reference to the ultimate targets of US department of energy for physisorption, temperature, pressure, and gravimetric density, we investigate the hydrogen storage capacity of Ti metal functionalized single walled carbon nanocones (SWCNCs), the preferable location of the metal, and metal clustering. We have considered the nH_2-Ti-CNC and nH_2-2Ti–CNC (n = 1–6) activated complexes with special attention to the characterization of reversible and irreversible hydrogen storage reactions and the thermodynamic capabilities of the highest hydrogen storage complex.

2. Computational details

The DFT calculations were performed by using Becke's three-parameter exchange functional (B3) with Lee Young Parr (LYP) correlation functional [14–17]. B3LYP correctly reproduces the thermo chemistry of many compounds including transition metal atoms [18–20]. The advantages of employing DFT calculations for hydrogen storage materials research may be summarized as the accuracy of computed thermodynamic quantities, the efficiency relative to experiment, and thermodynamic predictions of new functionalized nanostructures [21]. Full geometry optimizations without symmetry constraints were carried out for nH_2, CNC, Ti–CNC, nH2-Ti-CNC, and nH_2-2Ti–CNC (n = 1–6) at the B3LYP level of theory by using the 6-31G(d,p) basis set. This basis set uses Gaussian type functions (GTOs), adds d-type polarization functions to carbon, f-type polarization functions to titanium, and p-type polarization functions to hydrogen. The thresholds of geometry optimizations are: Maximum Force: 0.002500, RMS Force: 0.001667, Maximum Displacements: 0.010000, and RMS displacements: 0.006667. The convergence criteria of single point SCF energy calculations are: RMS density matrix = 1.00D-07, MAX density matrix = 1.00D-05, and energy = 1.00D-05.

The projected densities of states (PDOS), and Fermi levels were calculated by using the Gauss Sum 2.2.5 program [22]. All other calculations were carried out by using Gaussian 09 system [23]. The optimal geometries and frontier molecular orbitals were visualized by using the corresponding Gauss View 5.0 software.

3. Results and discussion

We constructed a CNC with disclination angle 180° and height 9 Å, consisting of 69 carbon atoms and 27 hexagonal rings. There are 24 bridge sites between hexagonal rings, in addition to 10 more associated with the dangling bonds at the CNC base, available for accommodating Ti atoms. The optimal geometries of CNC, Ti–CNC, $n$$H_2$–Ti–CNC, and $n$$H_2$–$Ti_2$–CNC ($n$ = 1–6) are shown in Fig. 1. The most stable site of Ti atom adsorption is the bridge site. The distances between the Ti atom and the nearest neighbor C atoms are 1.98 and 2.02 Å. The Ti adsorption energy of the functionalized CNC is defined as.

$$\Delta E_{ads.}(Ti) = E(Ti - CNC) - E(Ti) - E(CNC) \quad (1)$$

where E(Ti–CNC) is the total energy of the fully relaxed Ti–CNC, E(CNC) is the energy of the fully relaxed CNC, and E(Ti) is the energy of the free Ti atom. The adsorption energy of Ti atom −3.78 eV is significantly greater than the average adsorption energies of H_2 molecules ensuring the stability of the Ti–CNC complex in the event of H_2 molecule release, Table 1. The resulting dipole moment of 12.42 D from a Ti–CNC, compared to the case of 6.36 D for the

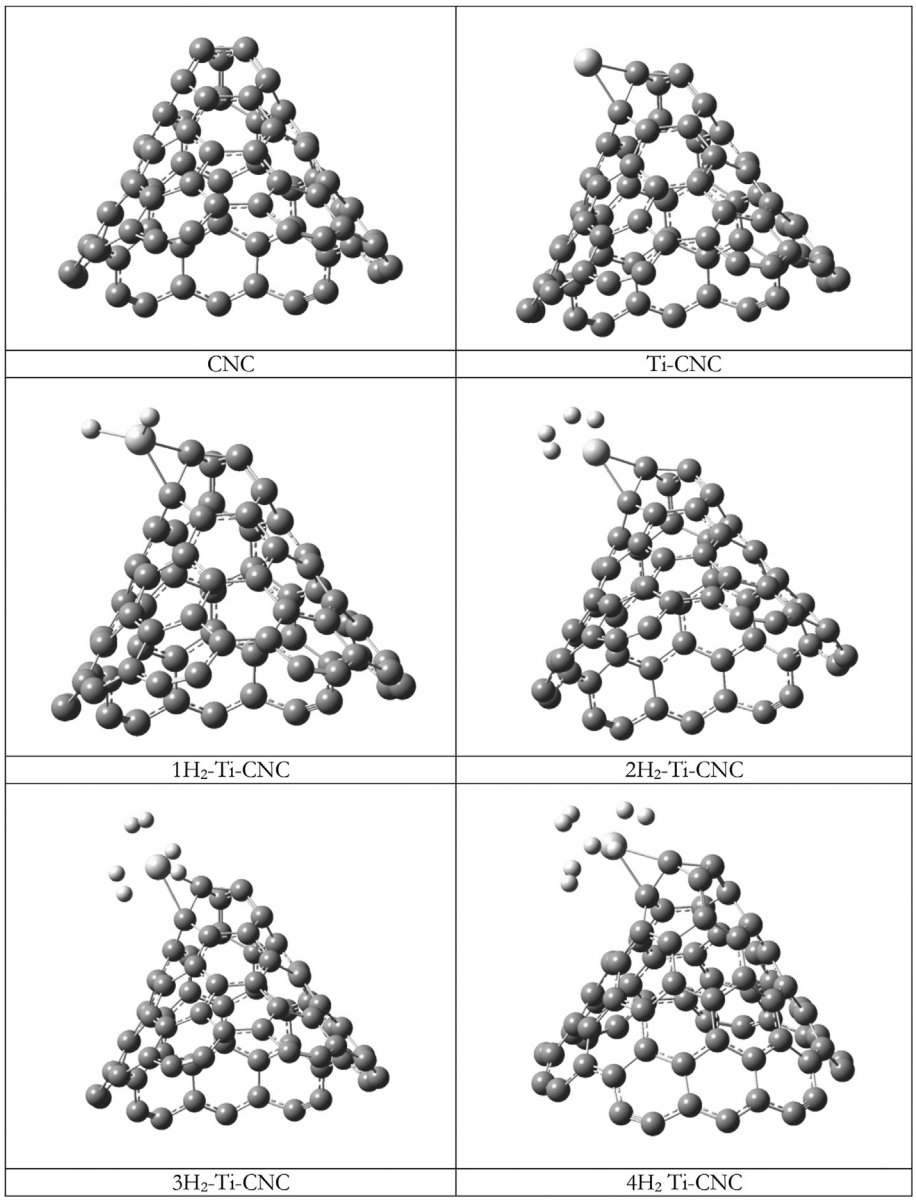

Fig. 1. The optimized geometries of CNC, Ti–CNC, nH_2-Ti-CNC ($n = 1$–6), Ti_2–CNC, nH_2-Ti_2-CNC (n = 2,4,6,8,10,12). For $144H_2$–Ti_{24}–CNC: six hydrogen moleculescould be adsorbed to a Ti atom in Ti_{24}–CNC. Carbon, titanium, and hydrogen are shown in grey, red, and white. (For interpretation of the references to color in this figure legend, the reader is referred to the web version of this article.)

pristine CNC, is sufficient to enhance the van der Waal's interaction between H_2 and CNC.

The average adsorption energy of H_2 over Ti_m-CNC is defined as.

$$\Delta E_{ads}(H_2) = [E(nH_2 - Ti_m - CNC) - nE(H_2) - E(Ti_m - CNC)]/n \quad (2)$$

where E($n$$H_2$–$Ti_m$–CNC) is the total energy of the fully relaxed nH_2–Ti_m–CNC, E(H_2) is the energy of an isolated relaxed hydrogen molecule, E(Ti_m–CNC) is the total energy of the fully relaxed Ti_m–CNC, (n) is the number of hydrogen molecules, and (m) is either 1 or 2. According to the precedent definitions, a negative value of $\Delta E_{ads}(H_2)$ corresponds to an exothermic adsorption.

The first H_2 molecule adsorbs on the bridge site between two hexagonal rings of Ti–CNC with a binding energy of −1.73 eV and an increased bond length of 2.91 Å compared to the original bond length of 0.74 Å. The adsorption is therefore dissociative, with Ti–H bond length of 1.71 Å, Table 1. The adsorption of the first H_2 molecule does not affect the distance between Ti and the nearest C and consequently does not affect the strength interaction between Ti and CNC. The mixed sp^2d hybridization of the Ti–C bonds seems to have strong repulsive effects on the adsorbed H_2 leading to elongation of the H–H distance 2.91 Å. The negative charges on the H_2 molecule and the negative charges on the nearest C atoms obtained from natural bond order (NBO) analysis ensure charge transfer from Ti to both of the H_2 molecule and the CNC. Since the hydrogen atoms of the adsorbed H_2 molecule have negative charges, the H_2 molecule can be considered as trapped by Ti cation via the charge polarization mechanism [24]. The charge on Ti is 0.49 and on the nearest neighbor carbons are −0.18 and −0.43. This indicates that Ti donates electrons to the neighboring C atoms on CNC where the d- orbitals of Ti atom overlap with the sp^2 orbitals of the Ti–C bonds to form the mixed sp^2d hybridization. This charge transfer behavior leads to Ti atom in cationic form and renders

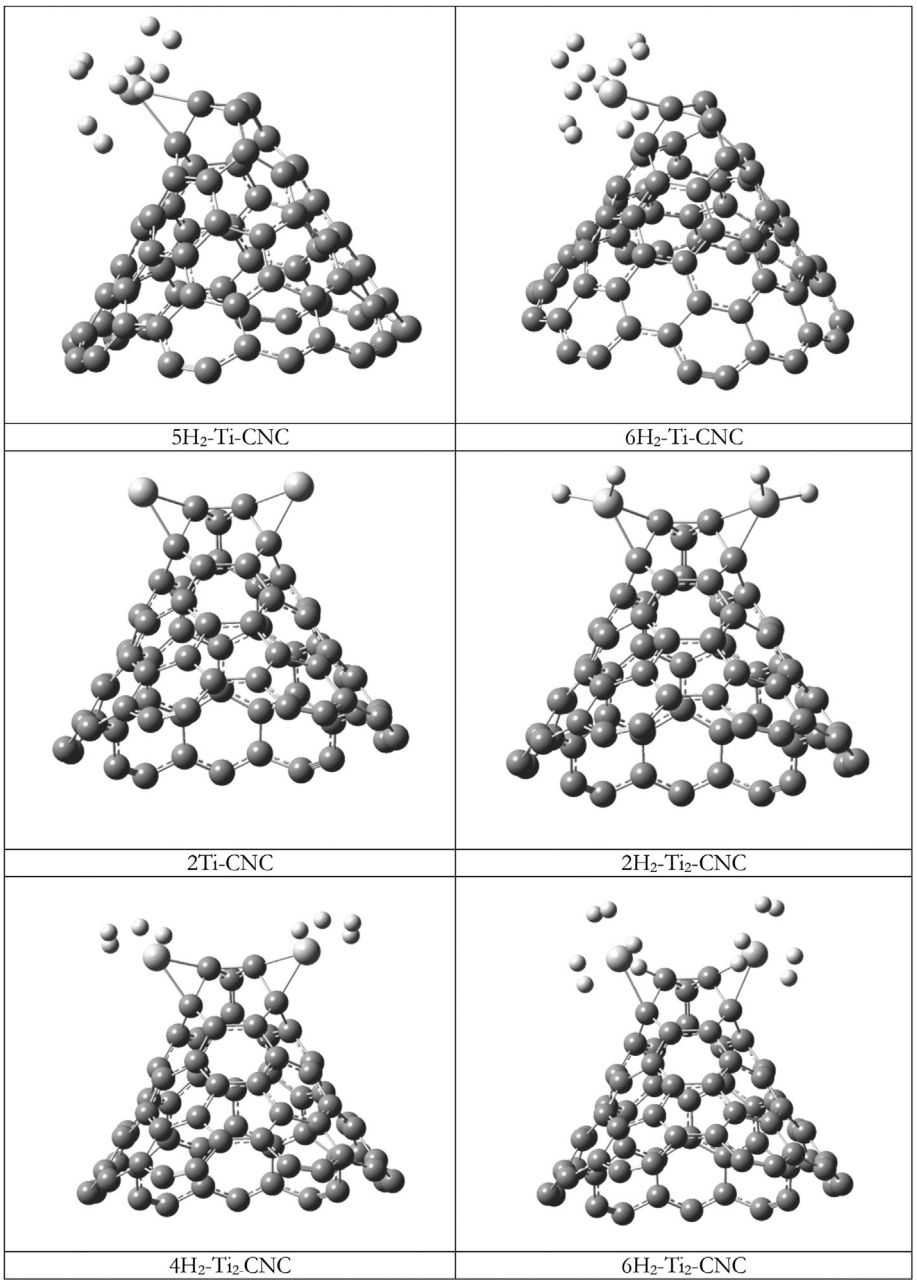

Fig. 1. (*continued*).

extensive hetero polar bonding between the Ti atom and the nearest C atoms, resulting in an increase in the H_2 molecule uptake. Moreover, the CNC approaching the positively charged Ti cation leads to loss of *d*- orbital degeneracy as the electrons of the CNC will be closer to some of *d*- orbitals while farther away from others. Thus *d*- orbitals closer to the CNC have a higher energy than those farther away. This results in the d- orbitals splitting in energy to reduce the total energy and stabilize the system as explained by ligand field theory [25]. Our NBO analysis of Ti–CNC and nH_2-Ti-CNC ($n = 1$–6) are shown in Table 2. The highest *d*- orbital energy levels are given between round brackets. These *d*- orbitals are therefore the most probable d- orbitals involved in the mixed sp^2d hybridization between C-sp^2 and Ti-*d*, and in the d-σ hybridization between Ti-*d* and H_2-σ or H_2-σ^*.

When more than one H_2 molecule is adsorbed on Ti–CNC, the average adsorption energies decrease to −0.74, −0.57, −0.45, −0.42, and −0.35 eV upon adsorption of the second to the sixth H_2 respectively. The Ti atom can therefore bind up to 6 H_2 molecules. While the average adsorption energies and charges of Ti atoms were decreasing functions of H_2 coordination number, the other structural parameters were not significantly affected.

The understanding of the distribution of frontier molecular orbitals (FMOs) around a nanostructure would be valuable to guideline the design of new functionalized materials for hydrogen storage. Frontier orbital isosurface plots of the substrate Ti–CNC complex are presented in Fig. 2. While strong localization of the highest occupied molecular orbital (HOMO) occurs on the Ti atom located at the tip area of the cone, strong delocalization of the lowest unoccupied molecular orbital (LUMO) occurs at the base

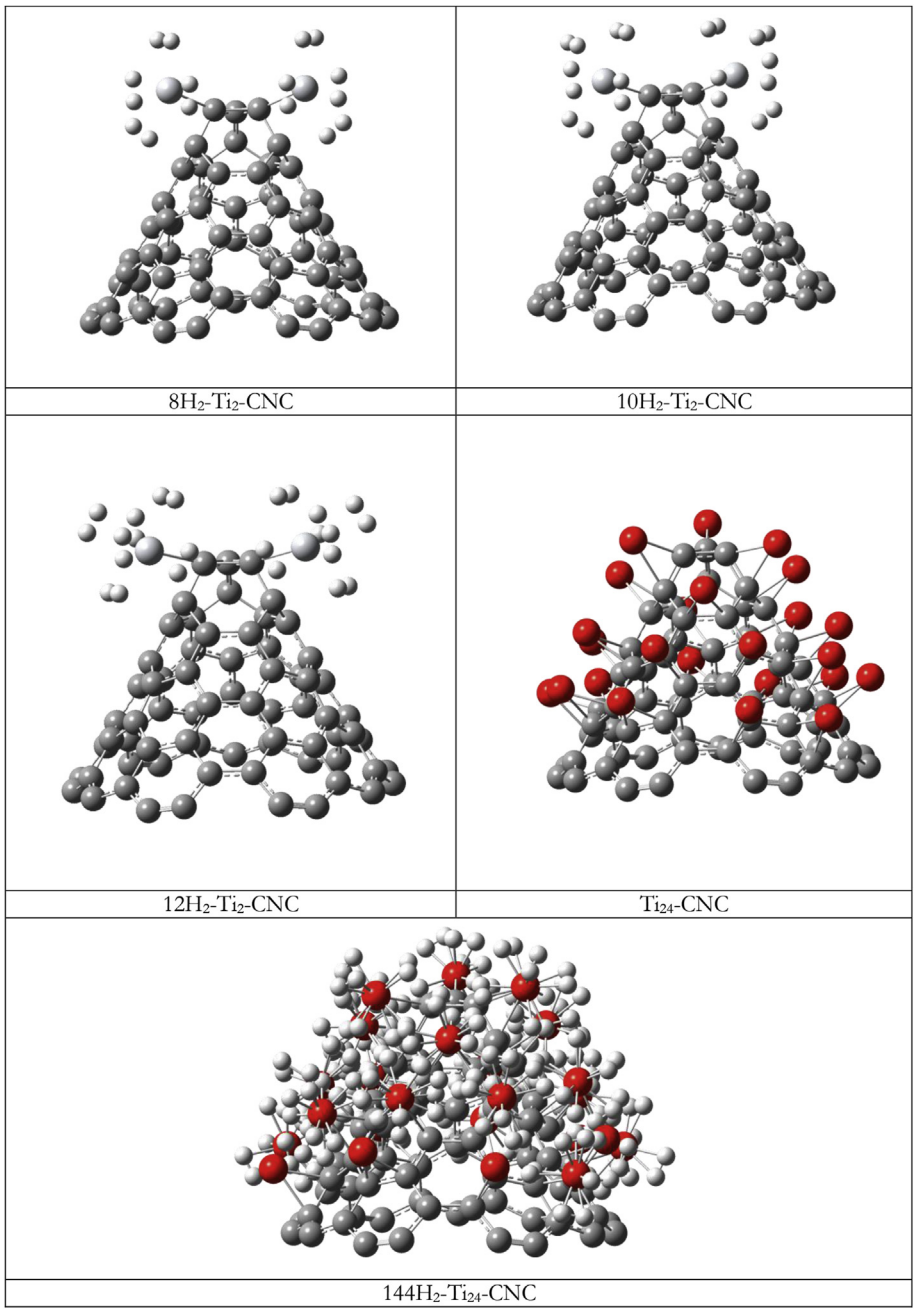

Fig. 1. (*continued*).

area. The strong localization of HOMO on Ti atom at the conical tip explains the enhanced adsorption interactions of nH_2 (−0.74 to −0.35 eV) relative to the DOE target of physisorption energies (−0.60 to −0.20 eV) and implies a significant flow of electron cloud across the interfaces between Ti and both of the adsorbed hydrogen and the outer surface of the cone.

To improve the hydrogen storage capacity, metal clustering should be avoided. We have examined systems containing two Ti atoms per CNC. The metal atoms are placed using the energetically most favorable location obtained from the optimization of a single atom adsorbed on CNC, namely, the bridge site between two hexagonal rings. Full geometry optimizations at the B3LYP/6-31g(d,p) level of theory were performed for the complexes nH_2-Ti_2-CNC (n = 2,4,6,8,10,12). The closest two bridge sites of the two Ti atoms at the cone tip are selected, and the average adsorption energies of 2, 4, 6, 8, 10, and 12 hydrogen molecules, geometric parameters, and the expected gravimetric hydrogen storage capacities are collected in Table 3. The gravimetric hydrogen storage capacity defined as the amount of hydrogen stored per unit mass of material was calculated from the relation.

$$\text{Wt \%} = \left(\frac{\text{nl } M_{H2}}{\text{nl } M_{H2} + \text{l } M_{Ti} + \text{m } M_C}\right) \times 100 \quad (3)$$

where n is the number of H_2 molecules adsorbed on each Ti atom, l is the number of Ti atoms, m is the number of carbon atoms, and M is the atomic or molecular weight. The distance between two Ti atoms at the nearest bridge sites of the cone tip (4.77–5.17 Å) is sufficiently large to avoid clustering of two adsorbed Ti atoms. Moreover, the interaction between Ti and CNC (−3.78 eV) is

Table 1
Structural and energetic properties of the optimized systems. All distances (d) are given in Å, average adsorption energies per H_2 ($\Delta E_{ads.}$) in eV, charges (Q) in a.u, and dipole moment (μ) in Debye.

	ΔE_{ads}	$d_{Ti\text{-}CNC}$	$d_{Ti\text{-}H}$	$d_{H\text{-}H}$	Q_{Ti}	Q_C	$Q_{H\text{-}H}$	μ
CNC						0.00		6.36
Ti–CNC	−3.78	1.98			0.49	−0.18		12.42
		2.02				−0.42		
$1H_2$–Ti–CNC	−1.73	1.97	1.71	2.91	0.88	−0.18	−0.22, −0.22	7.30
		2.03	1.71			−0.43		
$2H_2$–Ti–CNC	−0.74	1.97	1.81	0.88	0.70	−0.17	−0.020, −0.020	12.68
		2.06	1.85	0.89		−0.40	−0.030, −0.040	
$3H_2$–Ti–CNC	−0.57	1.98	1.84	0.81	0.62	−0.20	0.006, 0.005	14.49
		2.19	1.90	0.81		−0.29	0.020, −0.030	
			1.92	0.88			0.020, −0.030	
$4H_2$–Ti–CNC	−0.45	2.07	1.88	0.77	0.50	−0.12	0.050, −0.004	14.06
		2.08	1.88	0.80		−0.37	0.050, 0.020	
			1.92	0.81			−0.020, −0.004	
			2.09	0.84			−0.010, 0.030	
$5H_2$–Ti–CNC	−0.42	2.13	1.82	0.77	0.34	−0.12	0.015, 0.062	14.06
		2.17	1.90	0.79		−0.33	0.014, −0.012	
			1.93	0.80			0.039, 0.052	
			2.02	0.81			0.033, −0.013	
			2.10	0.88			0.033, 0.017	
$6H_2$–Ti–CNC	−0.35	2.10	1.90	0.76	0.14	−0.13	0.035,0.045	17.86
		2.25	1.90	0.77		−0.26	0.041,0.037	
			1.94	0.79			0.036,0.029	
			1.95	0.80			0.044,0.040	
			2.12	0.81			0.030,0.038	
			2.15	0.81			0.041,0.029	

stronger than the interaction between Ti and Ti–CNC (−3.50 eV). This in turn allows doping rules for high metal coverage. For nH_2-Ti_2-CNC ($n = 2,4$) complexes, the average adsorption energies of H_2 are −1.74 and −0.73 eV respectively, which are beyond the highest adsorption requirement (−0.60 eV). With these two configurations, the hydrogen storage capacities are expected to be 2.71% and 5.29%, respectively. For nH_2-Ni_2-CNC (n = 6,8,10,12) complexes, the average adsorption energies of H_2 are −0.55, −0.50, −0.42, and −0.35 eV, respectively and meet the DOE energy domain (−0.20 to −0.60 eV). With these four configurations, the hydrogen storage capacities are expected to be 7.73%, 10.04%, 12.24%, and 14.34%, respectively and exceed the ultimate target of DOE (7.5%). However, it must be mentioned that metal atoms may tend to aggregate into clusters when their concentration is large. Hence, the hydrogen storage capacities achieved in these ideal circumstances might be reduced once metal clustering occurs.

4. Interactions of $2H_2$ and $3H_2$ with Ti–CNC

Two types of interactions between nH_2 and Ti–CNC could be identified from Table 1 : (i) irreversible interactions between nH_2 (n = 1–2) and Ti–CNC (ii) reversible interactions between nH_2 ($n = 3$–6) and Ti–CNC. The irreversible interactions are outside the desirable energy window (−0.2 to −0.6 eV) recommended by DOE for practical applications, while the reversible interactions are inside. To characterize the nature of the two types of interactions, we considered the following theoretical descriptors (i) projected densities of states (ii) infrared and proton magnetic resonance spectra (iii) electrophilicity, and (iv) statistical thermodynamic stability, for the interactions of $2H_2$ and $3H_2$ with Ti–CNC.

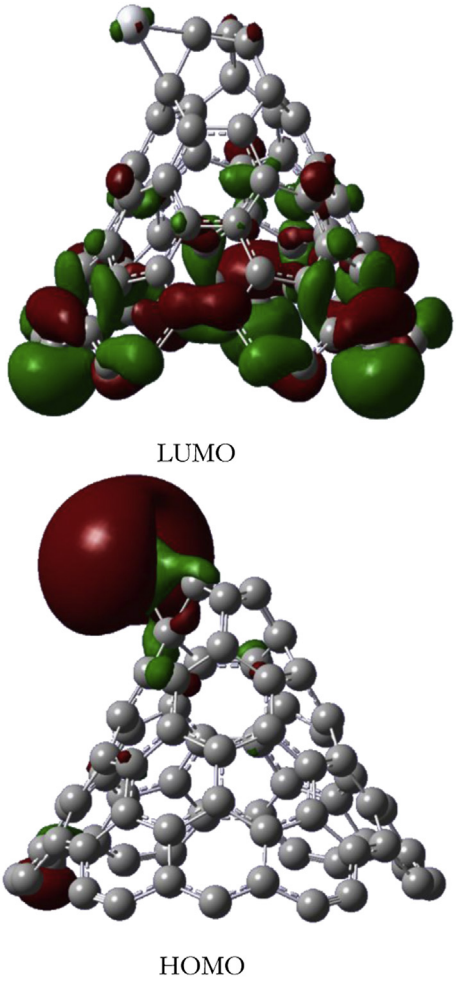

Fig. 2. Frontier molecular orbitals (FMOs) isosurface plots of Ti–CNC.

The projected densities of states (PDOS) for s- orbital of the H atom and *d*- orbitals of the Ti atom are shown in Fig. 3. The nature of Ti–H bonding can be explained from the analysis of PDOS plots. For $2H_2$–Ti–CNC complex, the bands of PDOS in the vicinity of the Fermi level (Region I) highlights that the hybridization of the Ti-*d* orbitals with the H_2 σ^* antibonding orbitals is responsible for the formation of Ti–H bond, where the binding state has a major contribution from Ti d- orbitals. In the energy range from −13 to −16 eV (Region II), the *d*- orbitals of Ti are hybridized with the σ orbitals of the hydrogen molecules, resulting in the H–H bond elongation, where the binding state has a major contribution from H_2-σ orbitals. With the help of NBO analysis, Table 1, we identify that the hydrogen atoms have negative charges (−0.02 to −0.04). This means that the d-orbitals of Ti donate electron to the H_2-σ^*

Table 2
Ti d- orbital energy (a.u) in the complexes Ti–CNC and nH_2-Ti-CNC (n = 1–6).

	Ti–CNC	$1H_2$–Ti–CNC	$2H_2$–Ti–CNC	$3H_2$–Ti–CNC	$4H_2$–Ti–CNC	$5H_2$–Ti–CNC	$6H_2$–Ti–CNC
d_{xy}	(−0.073)	−0.125	(−0.076)	−0.109	−0.122	−0.119	−0.078
d_{xz}	−0.118	−0.133	−0.119	−0.099	−0.105	−0.098	−0.099
d_{yz}	−0.084	(−0.113)	−0.096	−0.122	−0.099	−0.092	−0.125
$d_{x2\text{-}y2}$	−0.149	−0.125	−0.143	(−0.095)	(−0.080)	(−0.069)	−0.091
d_z^2	−0.112	−0.124	−0.107	−0.087	−0.088	−0.085	(−0.063)

Table 3
Average adsorption energies per H_2 (ΔE_{ads}), bond length between Ti and CNC d(Ti–CNC), bond length between Ti and H_2 d(Ti–H_2), H–H distance d(H–H), and the expected hydrogen storage capacity (wt%) of the complexes nH_2-Ti_2-CNC (n = 2,4,6,8,10,12). Complete surface coverage affords up to 34 Ti and 204 H_2.Energies are given in eV and lengths in Å.

	ΔE_{ads}	d(Ti–CNC)	d(Ti–H)	d(Ti–Ti)	d(H–H)	wt%
$2H_2$–Ti_2–CNC	−1.74	1.98, 2.03	1.71	4.85	2.93	2.71
$4H_2$–Ti_2–CNC	−0.73	2.00, 2.05	1.81, 1.82	5.17	0.88, 0.89	5.29
$6H_2$–Ti_2–CNC	−0.55	1.99, 2.18	1.83, 1.90, 1.92	4.81	0.81, 0.81, 0.89	7.73
$8H_2$–Ti_2–CNC	−0.50	2.03,2.31	1.84, 1.84, 1.88, 1.90	4.78	0.80, 0.81, 0.83, 0.87	10.04
$10H_2$–Ti_2–CNC	−0.42	2.03, 2.28	1.89, 1.90, 1.92, 1.94, 1.95	4.77	0.79, 0.80, 0.80, 0.81, 0.82	12.24
$12H_2$–Ti_2–CNC	−0.36	2.11,2.24	1.89, 1.90, 1.94, 1.95, 2.12, 2.13	5.10	0.76, 0.77, 0.79, 0.79, 0.81, 0.81	14.34

orbital of H_2. For $3H_2$–Ti–CNC complex, the general features of PDOS are different particularly in (Region II) where the H_2-σ orbitals of the hydrogen molecules hybridize with the d- orbitals of Ti. This hybridization is responsible for the charge transfer from H_2-σ orbitals to the vacant d- orbitals of Ti. The latter hybridization is confirmed by the NBO analysis of Table 1, which identifies that hydrogen atoms have positive charges. The present analysis reveals that not only the polarization mechanism but also the orbital hybridization between H-s orbitals and Ti-d orbitals act on the adsorbed H_2 molecules.

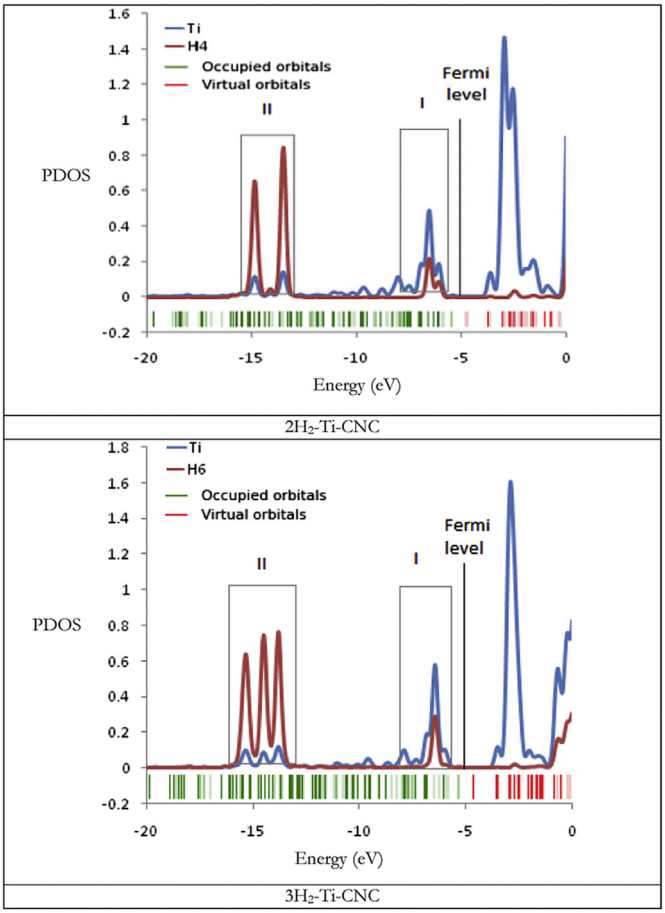

Fig. 3. Projected densities of states (PDOS) of $2H_2$–Ti–CNC and $3H_2$–Ti–CNC.

The infrared (IR) spectral analysis was carried out to search for the strongest vibrational modes of molecular hydrogen. The modes that are mixed with H_2 vibrations were not taken into account. The calculated infrared (IR) bands, force constants, and dipole strengths of hydrogen molecules in $2H_2$–Ti–CNC and $3H_2$–Ti–CNC are collected in Table 4. For $2H_2$–Ti–CNC, inspection of (IR) frequencies shows that all the bands undergo changes in positions and in intensities following the addition of one extra hydrogen molecule. Up shifts of the bands at frequency (2398 cm^{-1}) assigned to (H(71)-H(72)) with force constant (3.43 m Dyne/Å) and dipole strength (1993 10^{-46} esu^2 Cm^2) and at frequency (2444 cm^{-1}) assigned to (H(73)-H(74)) with force constant (3.56 m Dyne/Å) and dipole strength (4184 10^{-46} esu^2 cm^2) are observed under the effect of addition of one extra hydrogen molecule (H(75)-H(76)). The least IR frequencies and force constants are assigned to the hydrogen molecules (H(71)-H(72)), and the former effects are basically attributed to the interaction of the original $2H_2$ molecules with the one extra H_2, as well as the interaction of the H_2 molecules with Ti at the cone tip.

As far as the proton magnetic resonance (^{1}H NMR) is concerned, theoretical chemical shifts in (ppm) are calculated at the B3LYP/6-31g(d,p) level of theory for $2H_2$–Ti–CNC and $3H_2$–Ti–CNC complexes, Table 5. From the calculated data, H(71) to H(74) of the complex $3H_2$–Ti–CNC resonance at larger chemical shifts than those of the $2H_2$–Ti–CNC complex with respect to TMS at HF/6-31g(d) GIAO and TMS at B3LYP/6-311G(2d,p). The largest chemical shifts are assigned to H(73). However, the former trend is reversed for the calculated chemical shifts with no reference.

The formation energy (ε) is defined as the energy difference between the complex nH_2-Ti-CNC and the reaction components nH_2 and Ti–CNC.

$$\varepsilon = E(nH_2 - Ti - CNC) - E(nH_2) - E(Ti - CNC) \quad (4)$$

When $2H_2$ molecules are adsorbed, the formation energy is −1.470 eV. When $3H_2$ molecules are adsorbed, the formation energy increases to −1.704 eV. The formation energies are negative, thus hydrogen adsorption does not cost energy.

The ionization potential (I) and electron affinity (A) can be calculated from the relations.

$$I = E^{+1} - E^0 \quad (5)$$

$$A = E^0 - E^{-1} \quad (6)$$

where I and A are obtained from the total electronic energies E^{+1}, E^0, and E^{-1} of the cation, neutral, and anion forms of the complex nH_2-Ni-CNC at the neutral geometry [26,27].

In DFT the natural way to approximate electronegativity (χ) [28,29] and chemical hardness (η) [30,31] is to evaluate them directly from the calculated I and A.

$$\chi = -\mu = (I + A)/2 \quad (7)$$

$$\eta = I - A \quad (8)$$

The electrophilicity (ω) [32–34]is defined as.

$$\omega = \mu^2 / 2\eta \quad (9)$$

The total energy (E_{total}/E_h), formation energy (ε/eV), ionization

Table 4
The simulated infrared (IR) spectral bans of (H(71)-H(72) and H(73)-H(74)) in $2H_2$–Ti–CNC complex, and (H(71)-H(72), H(73)-H(74), H(75)-H(76)) in $3H_2$–Ti–CNC complex in the gas phase calculated at the B3LYP/6-31g(d,P) level of theory.

	Frequency (cm^{-1})	Force constant (m Dyne/Å)	Dipole strength (10^{-40} esu^2 cm^2)
$2H_2$–Ti–CNC H(71)-H(72)	2398	3.4266	1993
H(73)-H(74)	2444	3.5570	4184
$3H_2$–Ti–CNC H(71)-H(72)	2495	3.7069	4478
H(73)-H(74)	3291	6.4385	582
H(75)-H(76)	3366	6.7323	458

Table 5
The theoretical chemical shifts of ^{1}H NMR in (ppm) calculated at the b3lyp/6-31g(d,p) level of theory for $2H_2$–Ti–CNC and $3H_2$–Ti–CNC complexes.

	Atom	^{1}H NMR[a]	^{1}H NMR[b]	^{1}H NMR[c]
$2H_2$–Ti–CNC	H(71)	7.66	6.94	24.93
	H(72)	11.01	10.29	21.58
	H(73)	14.64	13.92	17.95
	H(74)	11.61	10.90	20.97
$3H_2$–Ti–CNC				
	H(71)	16.35	15.64	16.23
	H(72)	16.65	15.93	15.94
	H(73)	17.07	16.35	15.52
	H(74)	11.96	11.25	20.62
	H(75)	16.95	16.23	15.64
	H(76)	12.15	11.43	20.44

[a] with respect to TMS at HF/6-31g(d) GIAO.
[b] with respect to TMS at B3LYP/6-311+g(2d,p) GIAO.
[c] No reference.

potential (I/eV), electron affinity (A/eV), chemical hardness (η/eV), electronegativity (χ), and electrophilicity (ω/eV) of nH_2-Ti-CNC complexes (n = 2,3) are collected in Table 6. The $3H_2$–Ti–CNC complex is characterized by lower ionization potential (I), electron affinity (A), chemical hardness (η), electronegativity (χ), and electrophilicity (ω) relative to the $2H_2$–Ti–CNC complex. The hardness (η) of the complex $3H_2$–Ti–CNC is slightly smaller than that of the complex $2H_2$–Ti–CNC indicating a decrease in the rigidity of the $3H_2$–Ti–CNC complex thereby decreasing its stability. A good electrophile will be characterized by a high value of electrophilicity (ω). It is therefore evident that while the complex $2H_2$–Ti–CNC is better electrophile than $3H_2$–Ti–CNC, it is slightly more stable and less reactive than $3H_2$–Ti–CNC complex.

The Ti functionalized CNC shows a global minimum on the potential energy surface, suggesting that it is a dynamically stable structure at 0 K. To study the reactions of $2H_2$ and $3H_2$ with Ti–CNC, we calculated the changes of Gibbs free energy (ΔG) with temperature (T) of these two reactions from 100 to 600 K at 1 atm., Fig. 4 and Table 7. The thermodynamic properties of the complexes $2H_2$–Ti–CNC and $3H_2$–Ti–CNC can be calculated from the standard statistical mechanical equations to include the finite-temperature translational, rotational and vibrational energies. For example, the enthalpy (H_r) can be calculated as follows:

Table 6
The total energy (E_{total}/E_h), formation energy (ε/eV), ionization potential (I/eV), electron affinity (A/eV), chemical hardness (η/eV), electronegativity (χ/eV), and electrophilicity (ω/eV) of the complexes nH_2–Ti–CNC (n = 2,3).

n	E_{total}	ε	I	A	η	χ	ω
2	−3479.931	−1.470	4.479	4.045	0.434	4.262	20.938
3	−3481.118	−1.704	4.399	3.969	0.430	4.184	20.360

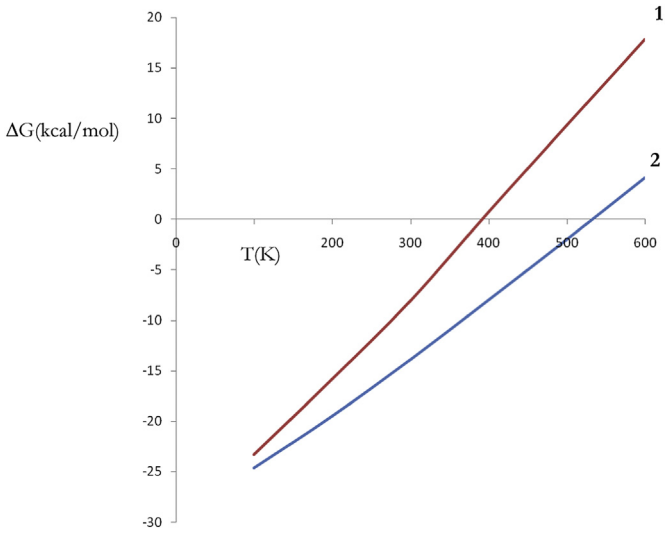

Fig. 4. Variations of Gibbs free energy (ΔG) with temperature (T) of the complexes **1**: $3H_2$–Ti–CNC and **2**: $2H_2$–Ti–CNC.

$$Hr = E_{elec.}(T = 0) + E_{vib.}(T = 0) + E_{vib.}(T) + E_{rot.}(T) + E_{tra.}(T) + PV \quad (10)$$

where $E_{elec.}(T = 0\ K)$ is the total electronic energy, $E_{vib.}(T = 0\ K)$ is the zero point vibrational energy (ZPVE) which is a linear sum of the fundamental harmonic frequencies, and $E_{vib.}(T)$, $E_{rot.}(T)$ and $E_{tra.}(T)$ are vibrational, rotational, and translational contributions, respectively. Similarly, the total entropy (S) can be calculated from the formula

$$S = S_{elec.} + S_{vib.} + S_{rot.} + S_{tran.} \quad (11)$$

where $S_{elec.}$, $S_{vib.}$, $S_{rot.}$, and $S_{tran.}$ are the electronic, vibrational, rotational, and translational terms. The change in the standard Gibbs free energy is given by

$$\Delta G = \Delta H_r - T\Delta S \quad (12)$$

where $\Delta H_r = H_{rP} - H_{rR}$ and $\Delta S = S_P - S_R$, or simply

$$\Delta G = GP - GR \quad (13)$$

Table 7
Temperature (T/K), Gibbs free energy ΔG (kcal mol^{-1}), enthalpy change ΔH (kcal mol^{-1}), entropy change ΔS (kcal mol^{-1} K), thermal energy E (K.cal mol^{-1}), and heat capacity at constant volume C_v (cal mol^{-1} K) of the complexes nH_2-Ti-CNC (n = 2,3).

T	n	ΔG	ΔH	ΔS	E	C_v
100	2	−24.59	−29.23	97.55	271.16	41.32
	3	−23.31	−30.18	98.74	282.67	43.49
200	2	−19.51	−30.35	147.94	278.62	109.19
	3	−15.84	−31.64	151.43	290.48	113.83
300	2	−13.87	−31.25	204.37	292.50	172.06
	3	−8.02	−32.26	211.39	305.29	179.62
400	2	−7.99	−31.88	263.38	312.89	226.33
	3	0.77	−33.19	271.38	326.07	234.17
500	2	−1.97	−32.31	319.06	337.72	268.55
	3	9.30	−33.48	328.91	351.73	277.35
600	2	4.14	−32.54	371.40	366.28	301.15
	3	17.86	−33.50	382.92	381.21	310.61

where P = product, and R = reactants. We have calculated the Gibbs free energy changes of the reactions

$$2H_2 + Ti{-}CNC \rightarrow 2H_2{-}Ti{-}CNC \quad (14)$$

and

$$3H_2 + Ti{-}CNC \rightarrow 3H_2{-}Ti{-}CNC \quad (15)$$

from 100 K to 600 K, in addition to enthalpy changes ΔH_r, entropy changes ΔS, thermal energies E_t, and heat capacities at constant volume C_v, Table 7. The polynomial regression

$$y = a_5x^5 + a_4x^4 + a_3x^3 + a_2x^2 + a_1x + a_0 \quad (16)$$

was then applied to the former reactions (14) and (15) from 100 to 600 K after replacing (y) by (T) and (x) by (ΔG). With residual sum of squares (rss = 0) the value of $\Delta G = 0$ occurs at $T = 532$ K for reaction (14), and $T = 392$ for reaction (15). In other words, reaction (14) reverses above 532 K, and reaction (15) reverses above 392 K. This implies that the complex $2H_2$–Ti–CNC tends to release all hydrogen above 532 K, while the complex $3H_2$–Ti–CNC tends to release all hydrogen above 392 K. As shown in Fig. 4 and Table 7, the ΔG values of the $3H_2$–Ti–CNC complex formation reactions are closer to $\Delta G = 0$ than those of the complex $2H_2$–Ti–CNC at all of the given temperatures. In other words, the higher is the hydrogen content of the starting cone Ti hydride, the lower is the temperature of hydrogenation. This can be explained by the relatively lower stability of the higher hydrogenated cone Ti hydride. The other statistical thermodynamic parameters also characterize the two types of interactions. Moreover, ΔH_r, ΔS, E_t, and C_v values of the irreversible interaction were always smaller than those of reversible interaction at the considered range of temperatures.

5. Interaction of $6H_2$ with Ti–CNC

It is possible to identify a range of reaction enthalpies that satisfy the ultimate DOE targets of temperatures and pressures through applications of van't Hoff relation. The former results, Tables 1 and 2, indicate that the highest hydrogen storage capacity reaction can be represented by the formation of the activated complex $6H_2$–Ti–CNC, where Ti can bind up to 6 hydrogen molecules with average adsorption energy of −0.35 eV per hydrogen molecule, and the gravimetric hydrogen storage capacity is expected to be as large as (14.34 wt%) in the ideal circumstances. To calibrate the thermodynamics of this reaction with the ultimate DOE hydrogen storage targets of (7.5 wt% H_2) for system gravimetric capacity, (−40/95–105 °C) for (min./max.) H_2 delivery temperature, and (0.3/1.2 MPa) for (min./max.) operating pressure, we calculated the corresponding changes of free energies (ΔG). To identify whether the activated complex $6H_2$–Ti–CNCs has promising thermodynamics (ΔH = 20–50 kJ mol^{-1} H_2) we also recorded (ΔH) values of the corresponding four T and P combinations. Moreover, to analyze the present thermodynamic data in the framework of surface coverage (θ), the Langmuir equation.

$$\theta = \frac{bP}{1 + bP} \quad (17)$$

where θ is the surface coverage, b is the absorption coefficient, and P is the pressure is combined with the van 't Hoff relation

$$\ln P = \frac{\Delta H}{RT} - \frac{\Delta S}{R} \quad (18)$$

where R is the universal gas constant and T is the temperature, to give the following expression for the surface coverage θ

$$\theta = \frac{P \exp\left(\frac{-\Delta H}{RT} + \frac{\Delta S}{R}\right)}{1 + P \exp\left(\frac{-\Delta H}{RT} + \frac{\Delta S}{R}\right)} \quad (19)$$

The (min./max.) temperature (T), (min./max.) pressure (P), free energy change (ΔG), enthalpy change (ΔH), and surface coverage (θ) are collected in Table 8. The ultimate targets of DOE are (−0.2 to −0.6 eV) for physisorption, (−40/95 to 105 °C) for (min.max.) temperature, (0.3/1.2 MPa) for (min./max.) pressure, and (7.5%) for wt%. As shown in Table 8, the interaction of $6H_2$ with Ti–CNC represented by the formation of the activated complex $6H_2$–Ti–CNC meets the ultimate targets of DOE at the minimum temperature (−40 °C/233.15 K) and maximum pressure (1.2 MPa/11.843 atm.) with surface coverage (0.941) where $\Delta G = -0.78$ kcal mol^{-1} and $\Delta H = -22.43$ kJ mol^{-1} H_2. The average adsorption energy per H_2 (−0.35 eV) satisfies the desirable energy window of DOE (−0.2 to −0.6 eV), the expected gravimetric hydrogen storage capacity (14.34%) in the ideal circumstances exceeds the ultimate target of DOE (7.5%), and the enthalpy change ($\Delta H = -22.43$ kJ mol^{-1} H_2) ensures the promising thermodynamics of hydrogen storage reactions (ΔH = −20 to −50 kJ mol^{-1} H_2).

Finally, Langmuir suggested that adsorption takes place through the mechanism Ag + S θ AS where A is a gas molecule and S is an adsorption site. The direct and inverse rate constants are k and k_{-1}. If we define surface coverage θ as the fraction of the adsorption sites occupied in the equilibrium, we have.

$$K = \frac{k}{k_{-1}} = \frac{\theta}{(1 - \theta)P} \quad (20)$$

where P is the partial pressure of the gas. For very low pressures ($\theta \approx KP$) and for high pressures ($\theta \approx 1$). Substituting the values of θ (0.941) and P (11.843 atm.) of the highest hydrogen storage capacity reaction in equation (20) gives the value ($K = 1.35$).

Experimentally, the most common method for determining enthalpy and entropy changes relies on equilibrium pressure-composition-temperature (PCT) data obtained from volumetric or gravimetric measurements. The procedure involves a series of experiments:(a) determination of a series of equilibrium concentration points at a given temperature via the step wise perturbation of pressure (b) construction of a full PCT curve from a series of kinetic measurements including a characteristic hysteresis loop (c) collection of analogous desorption PC isotherms at different temperatures with the flat plateau pressures (d)creation of the van't Hoff plot, where the slope and intercept of the line are related to the enthalpy and entropy changes of the reactions, respectively. Another commonly used method for experimental determination of thermodynamic properties is differential scaning calorimetry (DSC). It is a thermal analysis technique that measures the heat flow difference into a sample and a reference material as a function of temperature during a controlled temperature program. Complementary methods, such as temperature programmed mass spectrometry, X-Ray, neutron diffraction, infrared, Raman, and nuclear

Table 8
The (min./max.) temperature (T), (min./max.) pressure (P), free energy change (ΔG), enthalpy change (ΔH), and surface coverage (θ) of the highest hydrogen storage capacity reaction $6H_2$ + Ti–CNC = $6H_2$–Ti–CNC.

T(°C/K)	P(MPa atm^{-1})	ΔG(kcal mol^{-1})	ΔH(kJ mol^{-1} H_2)	θ
105/378.15	1.2/11.8430792	19.38	−23.88	7.33E-11
105/378.15	0.3/2.9607698	25.63	−23.88	4.45E-15
−40/233.15	1.2/11.8430792	−0.78	−22.43	0.941
−40/233.15	0.3/2.9607698	3.08	−22.43	0.004

magnetic resonance spectroscopy are also required to elucidate the underlying hydrogen desorption process [35–38].

To accelerate the discovery of hydrogen storage materials, a promising technique called “high throughput materials screening” has been developed. This technique couples the steps of synthesis (producing material), processing (modifying material to improve its thermodynamic and/or kinetic properties), and characterization [39]. As far as the present carbon nanocones are concerned, they are produced in an industrial process that decomposes hydrocarbons into carbon and hydrogen with a plasma torch having a plasma temperature above 2000 °C. This method is often referred to as Kvaerner Carbon Black & Hydrogen Process (CBH) and it is relatively “emission-free”, i.e., produces rather small amount of air pollutants. At certain, well optimized and patented conditions, the solid carbon output consists of approximately 20% carbon nanocones, 70% flat carbon discs and 10% carbon black [40]. Plasma-assisted decomposition of hydrocarbons has long been known and applied, for example, for production of carbon fullerene. Even if not optimized, it yields small amounts of carbon nanocones, which had been directly observed with an electron microscope already in 1994 [41].

6. Conclusions

An attempt has been made to guide materials development by translating vehicle operating constraints into thermodynamic constraints. Two types of reactions, namely reversible and irresversible, were characterized in terms of projected densities of states, infrared and proton magnetic resonance spectra, electrophilicity, and statistical thermodynamic stability descriptors. With reference to the ultimate targets of the department of energy for physisorption, gravimetric hydrogen storage capacity, minima and maxima of temperatures and pressures, and reaction enthalpies, the thermodynamics of the highest hydrogen storage capacity reaction were analyzed in some details. Carbon based materials have been identified as effective towards achieving promising performance and cost targets. They have shown to exhibit high gravimetric capacities and are on board reversible with facile kinetics. These gains are also expected from nanocones as members in the carbon based materials. However, modest volumetric capacities and poor thermodynamics of metal free hosts remain the key drawbacks. Consequently, discovering materials that exhibit all of the unique attributes required for hydrogen storage remains a challenge for materials research. We hope that present calculations suggest an approach to characterize and engineer new nanostructured materials as potential power sources.

References

[1] A.C. Dillon, K.M. Jones, T.A. Bekkedahl, C.H. Kiang, D.S. Bethune, M.J. Heben, Nature 386 (1997) 377–379.
[2] H. Tanaka, H. Kanoh, M. El-Merraoui, W.A. Steele, M. Yudasaka, S. Ijiima, K. Kaneko, J. Chem. Phys. B 108 (2004) 17457–17465.
[3] P. Matelloni, D.M. Grant, G.S. Walker, MRS Proc. 1216 (2009), http://dx.doi.org/10.1557/PROC-1216-W02-02, 1216-W02-02.
[4] M.-L. Liao, J. Nanopart. Res. 14 (2012) 837.
[5] A. Gotzias, H. Heiberg-Andersen, M. Kainourgiakis, Th Steriotis, Carbon 49 (2011) 2715–2724.
[6] Q. Wang, Q. Sun, P. Jena, Y. Kawazoe, ACS Nano 3 (2009) 621–626.
[7] T. Yildirim, S. Ciraci, Phys. Rev. Lett. 94 (2005) 175501.
[8] M. Samolia, T.J.D. Kumar, J. Phys. Chem. C 118 (2014) 10859–10866.
[9] A.S. Shalabi, S. Abdel Aal, M.M. Assem, W.S. Abdel Halim, Int. J. Hydrogen Energy 38 (2013) 140–152.
[10] S. Nachimuthu, Po-J. Lai, Jyh-C. Jiang, Carbon 73 (2014) 132–140.
[11] H. Xiao, S.H. Li, J.X. Cao, Chem. Phys. Lett. 483 (2009) 111–114.
[12] B. Chakraborty, P. Modak, S. Banerjee, J. Phys. Chem. C 116 (2012) 22502–22508.
[13] J. Yang, A. Sudik, C. Wolverton, D.J. Siegelw, Chem. Soc. Rev. 39 (2010) 656–675.
[14] A.D. Becke, J. Chem. Phys. 98 (1993) 5648–5653.
[15] S.H. Vosko, L. Wilk, M. Nusair, Can. J. Phys. 58 (1980) 1200–1211.
[16] A.D. Becke, Phys. Rev. 38 (1988) 3098–3100.
[17] C. Lee, W. Yang, R.G. Parr, Phys. Rev. B 37 (1988) 785–789.
[18] A. Ricca, C.W. Bauschlicher, J. Phys. Chem. 98 (1994) 12899–12903.
[19] T.V. Russo, R.I. Martin, P.J. Hay, J. Chem. Phys. 102 (1995) 8023–8028.
[20] P.E. Siegbahn, R.H. Crabtree, J. Am. Chem. Soc. 119 (1997) 3103–3113.
[21] C. Wolverton, D.J. Siegel, A.R. Akbarzadeh, V. Ozoliņš, J. Phys. Condens. Matter 20 (2008) 064228.
[22] N.M. O'Boyle, A.L. Tenderholt, K.M. Langner, J. Comput. Chem. 29 (2008) 839–845.
[23] M.J. Frisch, G.W. Trucks, H.B. Schlegel, G.E. Scuseria, M.A. Robb, J.R. Cheeseman, G. Scalmani, V. Barone, B. Mennucci, G.A. Petersson, H. Nakatsuji, M. Caricato, X. Li, H.P. Hratchian, A.F. Izmaylov, J. Bloino, G. Zheng, J.L. Sonnenberg, M. Hada, M. Ehara, K. Toyota, R. Fukuda, J. Hasegawa, M. Ishida, T. Nakajima, Y. Honda, O. Kitao, H. Nakai, T. Vreven, J.A. Montgomery, Jr, J.E. Peralta, F. Ogliaro, M. Bearpark, J.J. Heyd, E. Brothers, K.N. Kudin, V.N. Staroverov, T. Keith, R. Kobayashi, J. Normand, K. Raghavachari, A. Rendell, J.C. Burant, S.S. Iyengar, J. Tomasi, M. Cossi, N. Rega, J.M. Millam, M. Klene, J.E. Knox, J.B. Cross, V. Bakken, C. Adamo, J. Jaramillo, R. Gomperts, R.E. Stratmann, O. Yazyev, A.J. Austin, R. Cammi, C. Pomelli, J.W. Ochterski, R.L. Martin, K. Morokuma, V.G. Zakrzewski, G.A. Voth, P. Salvador, J.J. Dannenberg, S. Dapprich, A.D. Daniels, O. Farkas, J.B. Foresman, J.V. Ortiz, J. Cioslowski, and D.J. Fox, Gaussian, Inc., Wallingford CT, 2010.
[24] J. Niu, B.K. Rao, P. Jena, Phys. Rev. Lett. 68 (1992) 2277–2280.
[25] L.P. Zhang, P. Wu, M.B. Sullivan, J. Phys. Chem. C 115 (2011) 4289–4296.
[26] P.K. Chattaraj, S. Duley, J. Chem. Eng. Data 55 (2010) 1882–1886.
[27] R. Vijayaraj, V. Subramanian, P.K. Chattaraj, J. Chem. Theory Comput. 5 (2009) 2744–2753.
[28] P.K. Chattaraj, J. Indian Chem. Soc. 69 (1992) 173–183.
[29] R.G. Parr, R.A. Donnelly, M. Levy, W.E. Palke, J. Chem. Phys. 68 (1978) 3801–3807.
[30] R.G. Parr, R.G. Pearson, J. Am. Chem. Soc. 105 (1983) 7512–7516.
[31] R.G. Pearson, Chemical Hardness-applications from Molecules to Solids, Wiley-VCH, Weinheim, 1997.
[32] R.G. Parr, L. von Szentpá ly, S. Liu, J. Am. Chem. Soc. 121 (1999) 1922–1924.
[33] P.K. Chattaraj, U. Sarkar, D.R. Roy, Chem. Rev. 106 (2006) 2065–2091.
[34] P.K. Chattaraj, D.R. Roy, Chem. Rev. 107 (2007) PR46–74.
[35] T.P. Flanagan, W.A. Qates, Hydrogen in intermetallic compounds I, in: L. Schlapbach (Ed.), Topics in Applied Physics, Springer, Berlin, 1988, pp. pp.49–85.
[36] Aline leon (Ed.), Hydrogen Technology, Mobile and Portable Applications, Springer, Berlin, 2008, pp. 501–520.
[37] C.N. Park, S. Luo, T.B. Flanagan, J. Alloys Compd. 384 (2004) 203.
[38] P. Hohenberg, W. Kohn, Phys. Rev. 136 (1964) B864.
[39] R. Gremaud, M. Slaman, H. Schreuders, B. Dam, R. Griessen, Appl. Phys. Lett. 91 (2007) 231916.
[40] N. Stine Naess, Arnljot Elgsaeter, Geir Helgesen, D. Kenneth Knudsen, Sci. Technol. Adv. Mater. 10 (2009) 065002.
[41] Maohui Ge, Klaus Sattler, Chem. Phys. Lett. 220 (1994) 192.